RSC Advances

PAPER

View Article Online
View Journal | View Issue

Cite this: *RSC Adv.*, 2023, **13**, 24237

Photocatalytic performance of biochar-modified TiO_2 (C/TiO_2) for ammonia–nitrogen removal†

Jiawei Wang, [a] Guoqiao Wang,[a] Tian Yu,[a] Nengjie Ding,[a] Meicheng Wang[b] and Yao Chen *[a]

Biochar-modified TiO_2 (C/TiO_2) was prepared by a sol–gel method in this study to improve the photocatalytic capacity for ammonia–nitrogen (NH_3–N) removal from aqueous solutions. The results showed that biochar was successfully modified on TiO_2 and helped improve its photocatalytic performance for pollutant degradation. The removal capacity of ammonia–nitrogen on the synthesized photocatalyst performed well at pH 10 with 1 g L^{-1} C/TiO_2 under both 60 (12.25 mg g^{-1}) and 120 min (16.31 mg g^{-1}) irradiation (xenon lamp, AM1.5, 25 A). Characterization of C/TiO_2 through scanning electron microscopy-energy dispersive spectroscopy (SEM-EDS), Brunauer–Emmett–Teller (BET), X-ray diffraction (XRD), X-ray photoelectron spectroscopy (XPS), and Fourier-transform infrared spectrometry (FT-IR) analyses showed the successful introduction of biochar on TiO_2. SEM-EDS and BET analyses displayed that C/TiO_2 had a larger surface area and more pores than the raw materials. XRD spectroscopy illustrated that C/TiO_2 had typical characteristic peaks of anatase-TiO_2 and presented a good photocatalytic degradation performance. It was confirmed from XPS and FT-IR analyses that –COOH groups were present in C/TiO_2 and originated from biochar modification, and these enhanced the photocatalytic performance. Through radical quenching experiments, it was found that superoxide radicals ($^{\bullet}O_2^-$) played a dominant role in NH_3–N photocatalytic reactions with hydroxyl radicals ($^{\bullet}OH$) and valence band holes (h^+) playing a synergistic role. N_2 was the main degradation product after 6 h NH_3–N photocatalytic degradation, which was much larger than NO_3^-/NO_2^- (both almost undetected) and NH_3 (*ca.* 2 times lower than N_2). The new composite C/TiO_2 has potential for ammonia–nitrogen degradation in wastewater treatment and favorable for treating sewage sludge.

Received 6th June 2023
Accepted 29th July 2023

DOI: 10.1039/d3ra03789d

rsc.li/rsc-advances

1. Introduction

In recent years, water pollution has become and increasing concern attracting widespread attention. Population growth and industrial development have led to a range of serious environmental problems, including pollution from ever-increasing wastewater discharges. In 2020, 984-thousand tons of NH_3–N was discharged in China, which came from industrial, agricultural, and domestic wastewaters. Among this, more than 70% of NH_3–N originated from domestic wastewater (707-thousand tons).[1] An excess of NH_3–N in water can have detrimental consequences, including causing algal bloom, red tide, and the reproduction of algae, which can indirectly harm peoples' health.[2,3] It is thus essential to treat NH_3–N-contaminated water appropriately.

Blow-off, adsorption, and chemical precipitation are some common treatment methods for treating such waters, especially for low-concentration NH_3–N polluted wastewaters. However, there are some limitations to these methods. For example, free NH_3 can lead to air pollution, which is a health risk to people.[4] Adsorption is a reversible process, which can thus limit its application because of both efficiency and cost concerns.[5,6] Taking the deficiencies of traditional methods into consideration, it is crucial to explore new technologies.[7] Effectively changing NH_3–N into innocuous nitrogen is regarded by many as a perfect way to treat NH_3–N polluted wastewater.

Photocatalytic methods involve a newly developed advanced oxidation process, and have been proved to be the most promising technology nowadays due to their high efficiency, low toxicity, and environmental friendliness.[8,9] Semiconductor powders are widely used as photocatalysts.[10] Specifically, TiO_2 has notable advantages, including stable chemical properties, high photocatalytic activity, nontoxicity, strong oxidizing ability, and low cost.[11,12] It is the most used conventional photocatalyst and has shown good achievements in treating NH_3–N pollutants in water.[7] There are some research reports confirming that NH_3–N can be removed efficiently by TiO_2 photocatalysts from aqueous solutions.[4,13] TiO_2 has three main crystalline phases: anatase, rutile, and brookite. Among these, anatase TiO_2 shows

[a]*College of Architecture and Environment, Sichuan University, Chengdu 610065, China. E-mail: chenyao@scu.edu.cn; Fax: +86-28-8540-5613; Tel: +86-28-8540-3016*
[b]*China Construction Third Engineering Bureau Group Co., Ltd, Wuhan 430000, China*
† Electronic supplementary information (ESI) available. See DOI: https://doi.org/10.1039/d3ra03789d

the most prominent photocatalytic activity.[14] However, it still has some drawbacks. TiO_2 is limited by its large bandgap (E_g > 3.2 eV); thus, it can only be excited by about 7% energy of the solar light. Moreover, it is also limited by fast electron–hole recombination.[15,16] Thus, it is essential to overcome these difficulties to facilitate the use of TiO_2 as per its potential.

Researchers have devoted effort to modifying TiO_2, for instance by ion doping, semiconductor composite modification, noble metal deposition, *etc.* to enhance the performance of photocatalysts. Non-metal anion doping has been demonstrated to be an effective way to improve the photoactivity, with C-doping the most common one reported. Compared to traditional TiO_2, carbon-doped TiO_2 has a much narrower bandgap, which extends its photoresponse to visible light for enhancement of its photocatalytic activity and inhibits the generation of electron–hole pairs.[10,17,18]

Recently, various allotropes of carbon materials have been adopted to modify TiO_2. Biochar is a carbonaceous material with a high surface area, porous structure, low cost, and good sustainability.[19,20] There is a large amount of municipal sewage sludge generated as a by-product of wastewater treatment plants, which deserves urgent attention. The beneficial utilization of those solid wastes is an important and advanced way to solve environmental issues compared to traditional methods for its disposal, like incineration, landfill, *etc.* Thus, transforming sewage sludge into biochar was attractive and feasible.[21] Biochar provides a versatile and efficient platform for the synthesis of functionalized carbon materials. Compared to conventional activated carbon, biochar performs much better in TiO_2 modification due to its greater number of inner elements, such as N, S, and more abundant surface functional groups like carbonyl and carboxyl groups.

In our study, the feasibility of biochar-modified TiO_2 for the photocatalytic decomposition of NH_3–N in wastewater was evaluated. Dehydrated sewage sludge-based biochar was used to prepare a C/TiO_2 composite photocatalyst through a sol–gel method. The removal capacity of NH_3–N was studied under different operations. SEM-EDS, BET, XRD, XPS, and FT-IR characterizations of the photocatalysts were performed and discussed in detail for better understanding the performance of the biochar-modified TiO_2 for NH_3–N removal. It was hoped it would achieve a combination of adsorption and photocatalytic activity for NH_3–N treatment, considering that various elements in biochar have integrated effects on photocatalytic reactions compared to a single element material. Moreover, Li Zhang *et al.* proved that with the help of adsorptive biochar, pollutants could easily gather around the photocatalysts and be efficiently removed by the accelerated photocatalytic reactions.[22] It was expected that this would be helpful for the innovative modification of titanium dioxide for use as a photocatalyst to realize resource utilization through NH_3–N degradation.

2. Materials and methods

2.1 Preparation of C/TiO_2 photocatalyst

Dehydrated sewage sludge from a local municipal wastewater treatment plant (WWTP) was collected as the raw material to prepare the biochar, as described in our previous work, for further utilization.[23,24]

First, 20 mL ethanol and 7.2 mL butyl titanate were mixed in a container and shaken for 0.5 h (450 rpm). Hydrochloric acid was then added into the solution and stirred together for 0.5 h in order to maintain an acidic condition. Next, 0.2 g biochar powder was added to the above solution and stirred (450 rpm) for another 0.5 h to ensure a thorough mixing. Finally, 5.6 mL deionized water and 4.4 mL ethanol were added to the solution and kept stirring until gel formation.

After achievement of the wet gel, it was sealed for 24 h and then put into an oven (105 °C) for 12 h drying. The xerogel was subsequently ground into powder, and then calcined in a tubular furnace at 500 °C (heating rate: 2 °C min^{-1}) for 4 h in a nitrogen atmosphere. After that, the manufactured product was taken out to cool down to room temperature. The product was washed by deionized water several times and dried to obtain the final compound, named as C/TiO_2, with a TiO_2 and biochar composition.[23]

2.2 Experiments

Ammonium chloride (NH_4Cl) was dissolved in deionized water to prepare NH_3–N bulk solution. As illuminated in Fig. S1 (ESI†), a high-pressure xenon lamp (PL-XQ 500 W) was used as the light source. The details of the xenon lamp are provided in the ESI (Fig. S1†). Here, 100 mL NH_3–N solution (50 mg L^{-1}) and a certain amount of the composed photocatalyst were mixed in a 200 mL sealed beaker with magnetic stirring (450 rpm). An outer circulation cooling water system was applied to maintain the reaction system under room temperature. Fig. S2† shows a schematic diagram of the reaction system reaction (see the ESI†). At designed time intervals, samples were taken out and filtered, and the NH_3–N concentration of the supernatant was analyzed *via* a standard method. Excessive doses of dilute sulfuric acid and phenolphthalein solution were provided for tail gas treatment, and the mass of ammonia was determined by the weight deviation after exhaust adsorption.

Quenching agents were added into a series 100 mL NH_3–N (50 mg L^{-1}) solutions with 1 g L^{-1} C/TiO_2 under a high-pressure xenon lamp (AM1.5, 25 A) for 1 h stirring (450 rpm). Samples were taken out and filtered every 20 min, and the concentrations of various nitrogen contents in the supernatant were determined in accordance with standard methods (see the ESI†).

NH_3–N removal capacity was calculated by the following equation.

$$X_1 = V \times (C_0 - C_1)/M \quad (1)$$

where C_0 and C_1 (mg L^{-1}) are the initial NH_3–N concentration and NH_3–N concentration at reaction time t (min), respectively, V is the volume of the solution (L), M is the weight of the photocatalyst or biochar (g), and X_1 is the NH_3–N removal capacity (mg g^{-1}).

Determination of the NH_3–N concentration was done in accordance with the standard method HJ 535-2009 (Nessler's reagent spectrophotometry). The standard method HJ/T346-

2007 (water quality – determination of nitrate–nitrogen – ultraviolet spectrophotometry method) and GB 7493-87 (water quality – determination of nitrogen(nitrite) – spectrophotometric method) were used to determine the concentration of NO_3^- and NO_2^-, respectively. A PHS-4 pH meter (Shanghai INESA Scientific Instrument Co., Ltd) was used to measure the pH values for the samples.

The commercial titanium dioxide (anatase-TiO_2) adopted in this work was analytical grade powder (≥99.0%) and was purchased from Kelong Chemical Reagent Co., Ltd. All other chemicals and reagents used to prepare the photocatalysts were analytical grade and provided by Kelong Chemical Reagent Co., Ltd, as well. Propan-2-ol (IPA) and potassium iodide (KI) were applied as quenching agents and both were analytical grade and obtained from Kelong Chemical Reagent Co., Ltd. Nitro blue tetrazolium (NBT) was applied as a quenching agent and was purchased from Shanghai Aladdin Biochemical Technology Co., Ltd.

All experiments were carried out twice under identical conditions, and the results were collected as the mean values.

2.3 Characterization

SEM-EDS was used to determine the surface morphology of the raw materials and the composed photocatalyst. This was completed at the Analytical and Testing Center of Sichuan University using a JSM-7500F field emission scanning electron microscope (JEOL): acceleration voltage of 0.1 kV to 30 kV, resolution of 1.0 nm (15 kV), 1.4 nm (1 kV), and magnification of ×25–×8 00 000. The BET surface area and pore volume of the samples were measured using a TriStar II 3020 Version 3.02 (Micromeritics Instrument Corporation).

X-Ray diffraction spectroscopy (XRD, EMPYREAN, PANalytical B.V.) was used for phase identification with Cu Kα radiation at 1.54 Å (X-ray wavelength) from 10° to 70° (2θ). The surface element properties were analyzed by X-ray photoelectron spectroscopy (XPS, XSAM800, Kratos) using an Al Kα source. The functional groups of the materials were detected by Fourier-transform infrared spectroscopy (FT-IR, FNicolet 6700, Thermo Elemental) within the range 4000–400 cm^{-1}.

3. Results and discussion

3.1 NH_3–N removal

The photocatalytic performance of the biochar, commercial TiO_2, and the composed C/TiO_2 were investigated by adding 1 g L^{-1} of biochar, TiO_2, or C/TiO_2 into a series of 100 mL of 50 mg L^{-1} NH_3–N solutions under the dark and photocatalytic conditions, respectively. The dark groups were carried out under constant stirring (450 rpm) without lighting for 1 and 2 h, while the photocatalysis groups were analyzed with fully mixing under xenon lighting (AM1.5, 25 A) for 1 and 2 h. Also, control group 1 was a blank solution without any adsorbent under dark condition and control group 2 was a blank sample without any photocatalyst under irradiation.

As shown in Fig. 1, the removal capacity of NH_3–N was much different under the varied reaction conditions. Under the dark condition, there was insignificant NH_3–N removal by all the products (biochar, commercial TiO_2, and C/TiO_2), namely lower than 5 mg g^{-1} for 1 h and 7 mg g^{-1} for 2 h. Compared with the results for control group 1, none of them presented adsorptive capacity for NH_3–N removal. The slight decrease in NH_3–N concentration under the dark conditions was mainly due to the solution stirring and blowing off the ammonia during the experiments for the control groups. Febio Dalanta *et al.* found there was approximately no NH_3–N adsorption on TiO_2,[25] which was the same as our experimental results. While under irradiation, compared to control group 2, both the commercial TiO_2 and C/TiO_2 photocatalysts performed well in NH_3–N degradation, with a similar high removal capacity. The NH_3–N removal capacity was *ca.* 12 mg g^{-1} for 1 h and 16 mg g^{-1} for 2 h on C/TiO_2, respectively, which were slightly higher than on commercial TiO_2. C/TiO_2 had a much better NH_3–N removal capacity almost 3 times higher than the one in the dark conditions. It was demonstrated that with external illumination, the degradation ability of C/TiO_2 on NH_3–N was effectively enhanced by photocatalysis. In terms of the preparation and beneficial utilization of waste, the biochar-modified TiO_2 has great potential for use in ammonia–nitrogen wastewater treatment.

Taking the application of the composite photocatalysts into consideration, natural waters from Jiang'an River and Mingyuan Lake in our campus were collected and tested (Experiment details are provided in the ESI†). The NH_3–N removal capacity was *ca.* 6.58 mg g^{-1} for the Jiang'an River sample and 7.89 mg g^{-1} for the Mingyuan Lake sample on C/TiO_2, respectively, which were similar to the ones achieved by the commercial TiO_2 (7.03 mg g^{-1} for Jiang'an River water and 7.52 mg g^{-1} for Mingyuan Lake water, respectively). Actually, the NH_3–N removal capacities on C/TiO_2 and TiO_2 were relatively lower than the one for the synthetized NH_3–N wastewater in the lab due to the complexity of the natural water bodies. The results showed the great potential for practical use of C/TiO_2 for NH_3–N removal from natural water resources.

Table 1 shows the removal capacity of NH_3–N on different photocatalysts in similar studies. As listed in Table 1, the photocatalytic effect C/TiO_2 for NH_3–N removal was superior to most products. Specifically, the NH_3–N removal capacity on C/TiO_2 was 16.31 mg g^{-1} in our study and was obviously higher than the other photocatalysts under the same irradiation time (2 h). Compared to B–SiO_2@TiO_2 (100 : 5) at 150 min and Cu/TiO_2 at 180 min, C/TiO_2 had an approximate efficiency for NH_3–N removal in a relatively short reaction time (120 min). In comparison with other photocatalysts, C/TiO_2 has prominent advantages due to its simple operation, waste sustainable utilization, easy availability, as well as high efficiency for NH_3–N degradation.

3.2 Photocatalysis

3.2.1 Effect of the lighting. The wavelength and luminous energy are different for UV light, visible light, and sunlight. Thus, the effects of the light source and irradiation intensity on NH_3–N removal were discussed in the study. Three light filters

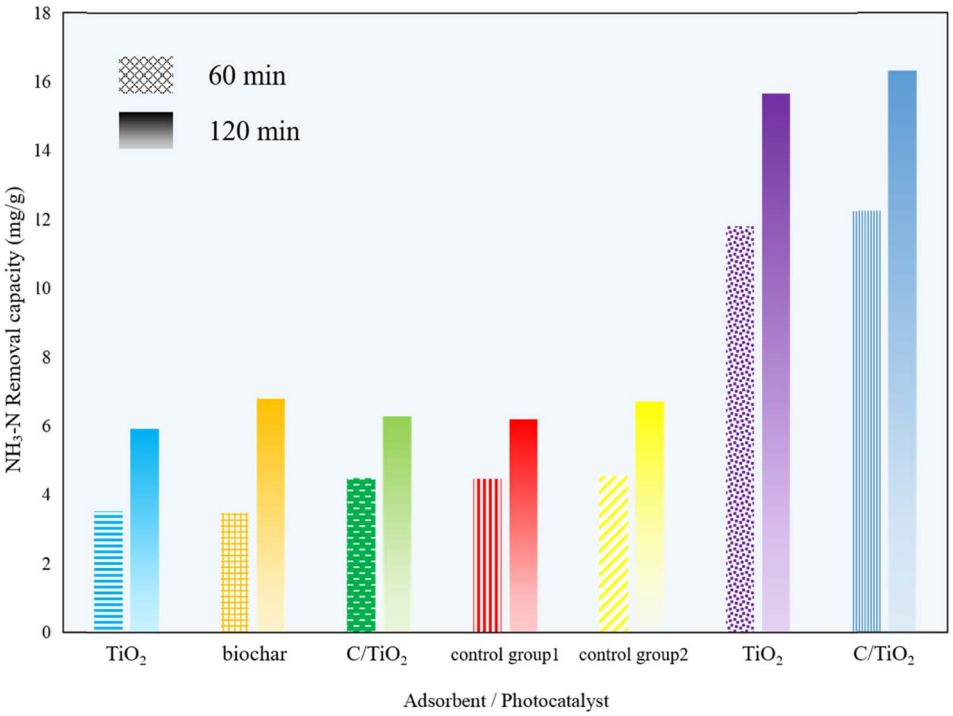

Fig. 1 NH_3–N removal capacity under different reaction condition times (AM1.5, 25 A, 1 g L^{-1} of photocatalyst, pH 10.0, C_0 = 50 mg L^{-1}).

Table 1 Degradation of NH_3–N on different photocatalysts

Photocatalyst	Light source	Light power (W)	pH	Irradiation time (min)	Removal capacity (mg g^{-1})	Reference
C/TiO_2	Simulated sunlight	500	10.0	120	16.31	This study
TiO_2/MPVA-Alg	UV	250	10.5	120	1.575	Zendehzaban *et al.*[26]
TiO_2/perlite	UV	125	11.0	120	14.01	Shavisi *et al.*[27]
B–$SSiO_2$@TiO_2 (100 : 5)	Visible light	100	8.0	150	18.36	Zhou *et al.*[28]
Cu/TiO_2	Sunlight	—	—	180	17.50	Wang *et al.*[29]

(AM1.5, UV cut-off at 400 nm, UV) were installed on a xenon lamp to get different wavelength conditions, which were simulated sunlight (0–2500 nm), visible light (400–760 nm), and ultraviolet light (250–400 nm), respectively. The light intensity was set between 50 mW cm^{-2} (low) to 100 mW cm^{-2} (high) *via* adjusting the current intensity from 15–25 A. Light source experiments were carried out with a current intensity at 25 A, while different luminous energy experiments were adjusted between 15–25 amp under simulated sunlight (AM1.5) operation.

As shown in Fig. 2a, there was a remarkable light-utilization ability of C/TiO_2 for NH_3–N degradation. The removal ability through NH_3–N degradation by C/TiO_2 under the three kinds of light sources increased with prolonging the lighting time, and presented different performances. The photocatalytic reaction excited under simulated sunlight displayed the most prominent capacity compared with the other two light sources. After 60 min, the NH_3–N removal capacity under simulated sunlight was up to 12.25 mg g^{-1}, which was higher than both that under UV and visible light.

As is widely known, TiO_2 can be efficiently excited by the ultraviolet part of sunlight, while an absorption band change can be subsequently found in the composed material.[30–33] Here, C/TiO_2 could effectively absorb ultraviolet light, and also efficiently utilize the relatively long wavelength of visible light. Sunlight represents the sum energy of visible light and ultraviolet light, which made the total light energy absorbed by C/TiO_2 greater than that for ultraviolet light, and led to the improved light-utilization efficiency and removal capacity of NH_3–N. Thus, C/TiO_2 has advantages in light utilization and photocatalysis compared to the common TiO_2.

As illuminated in Fig. 2b, the reaction was conducted under a xenon lamp (AM1.5), while the luminous power was adjusted within 15–25 A (300–500 W, over a light intensity range of 50–100 mW cm^{-2}). With the increment in light power, the NH_3–N treatment efficiency by C/TiO_2 also increased. After 60 min, the NH_3–N removal capacities under the low, medium and high light intensity power were 9.34, 10.87, and 12.25 mg g^{-1}, respectively. With the enhancement of the light intensity, more effective photons were generated and the light penetration

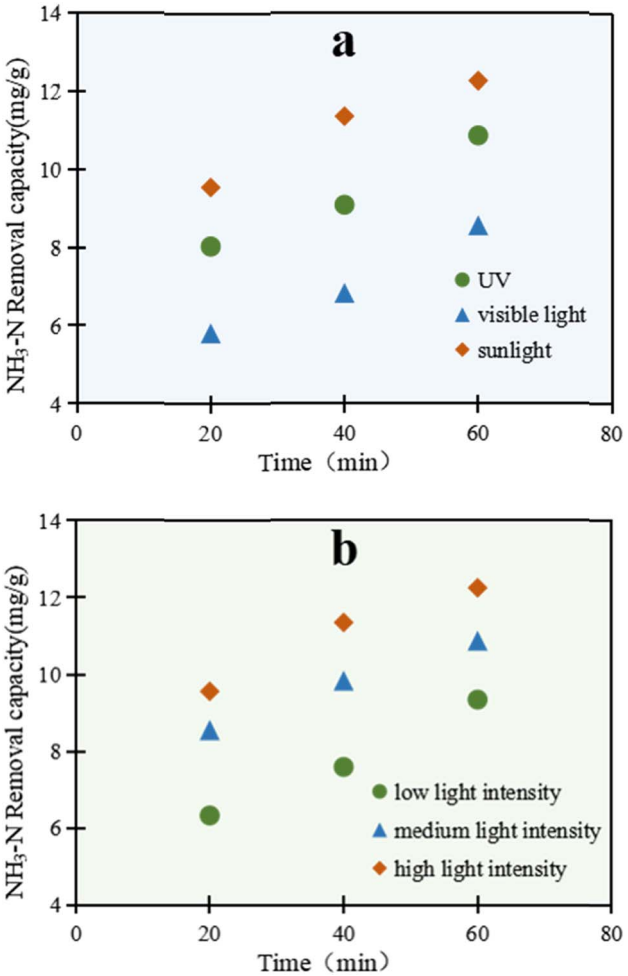

Fig. 2 NH_3–N removal capacity under different irradiation intensities by the C/TiO_2 photocatalysts, with varying the (a) light source (25 A, 1 g L^{-1} C/TiO_2, pH 10.0, $C_0 = 50$ mg L^{-1}); and (b) light intensity, from a low to high intensity of 50–100 mW cm^{-2} (AM1.5, 1 g L^{-1} C/TiO_2, pH 10.0, $C_0 = 50$ mg L^{-1}).

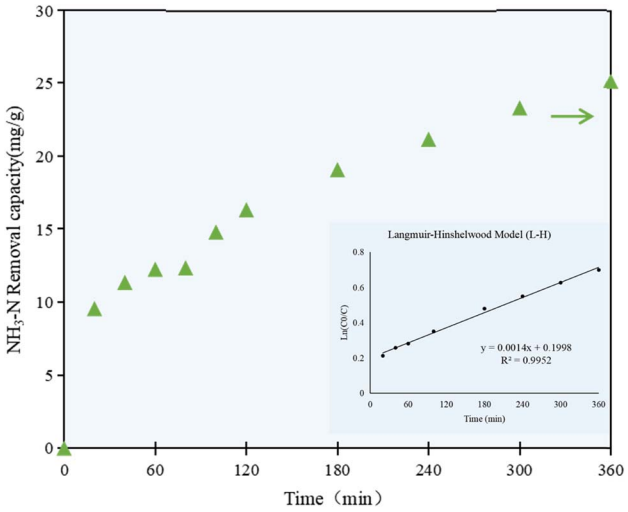

Fig. 3 NH_3–N removal capacity at different irradiation times by the C/TiO_2 photocatalysts (AM1.5, 25 A, 1 g L^{-1} C/TiO_2, pH 10.0, $C_0 = 50$ mg L^{-1}).

ability was improved too. Meanwhile, the probability of electron transition was strengthened, with a higher generation of active free radicals on the C/TiO_2 surface. Consequently, the photocatalytic degradation capacity for NH_3–N increased. Moreover, the increased photons made more NH_3–N molecules absorb light energy and become activated, which was conductive to the photocatalytic reactions. However, with further increasing the light intensity, the NH_3–N photodegradation by C/TiO_2 became stable and showed insignificant further change due to the limitation of the light quantum efficiency. Here, the probabilities of collision between activated electrons and holes were greatly enhanced and consequently led to annihilation under strong light irradiation; however, when the amount of C/TiO_2 was constant, the number of electron–hole pairs did not increase with the increment in the number of photons.[34]

3.2.2 Effect of the irradiation time. First, 1 g L^{-1} C/TiO_2 was added into 100 mL NH_3–N solution (50 mg L^{-1}, pH 10.0), and the photocatalytic reaction was carried out under a xenon lamp (AM1.5, 25 A) for 6 h. Samples were taken out and filtered at set time intervals, and the NH_3–N concentration of the supernatant was analyzed.

As shown in Fig. 3, the NH_3–N removal capacity by the C/TiO_2 photocatalyst increased with prolonging the irradiation time, while the NH_3–N concentration in the solution decreased simultaneously. The NH_3–N removal capacity increased rapidly to 12.25 mg g^{-1} in the first 60 min, and then had a continuing and stable increment of 11.05 mg g^{-1} after 5 h reaction, while it was still slightly raised by *ca.* 2.0 mg g^{-1} at 6 h of reaction. A high NH_3–N removal capacity was achieved at the end of the experiment, which was more than 2 times higher than that at 1 h reaction.

The NH_3–N removal capacity on C/TiO_2 showed a rapid growth phase in the first 60 min, then increased steadily in the following 300 min, which proved that the change in the removal capacity was continuous and stable with prolonging the irradiation time. While the photocatalytic activity on C/TiO_2 gradually increased with the progression of the reaction, the NH_3–N concentration decreased steadily and reached a plateau due to the limited pollutant available. Taking energy-saving and efficiency into consideration, further experiments were performed under light for 60 min.

According to the concentration of ammonia–nitrogen in the solution at the set irradiation time intervals, the kinetic model for the photocatalytic reaction was studied. As shown in Fig. 3, the correlation coefficient R^2 was calculated to be 0.9952, which proved that the photocatalytic reaction of C/TiO_2 well fitted the Langmuir–Hinshelwood model (L–H). The L–H theory is based on the principles of adsorption and desorption, and it represents a multiphase catalytic mechanism where surface reactions are the controlling steps for the adsorbed molecules. According to the experimental data and the kinetic model, the photocatalytic reaction occurred on the surface of the catalyst, while the rate of the catalytic reaction depended on the reaction between the surface-adsorbed molecules, and the adsorption and desorption processes were in a dynamic equilibrium state.[35]

3.2.3 Effect of the catalyst dosage. The dosage of a photocatalyst plays a vital role in the photocatalytic reaction. Here, 0.5–2.0 g L^{-1} C/TiO_2 was added into 100 mL of 50 mg L^{-1} NH_3–N solution (pH 10.0), and the photocatalytic reaction was carried out under a xenon lamp (AM1.5, 25 A) for 1 h. During the reaction, samples were taken out and filtered at set time intervals, and the NH_3–N concentration of the supernatant was analyzed *via* the standard method.

The NH_3–N photocatalysis removal capacity results with varying the C/TiO_2 dosage (0.5–2.0 g L^{-1}) are shown in Fig. 4. It was confirmed that the NH_3–N removal capacity was enhanced with the C/TiO_2 dosage increasing, and obviously increased from 9.59 mg g^{-1} to 12.25 mg g^{-1} as the C/TiO_2 dosage increased from 0.5 to 1.0 g L^{-1}, while it showed an insignificant increment when the C/TiO_2 dose was increased further to 1.5 and 2.0 g L^{-1}.

The highest NH_3–N degradation was obtained with 2 g L^{-1} photocatalyst due to the larger contact surface area, more photocatalytic activity points, and more active free radicals produced. Otherwise, the NH_3–N removal capacity would be affected by the continuous dosage increment. Though a large number of photocatalytic activity sites would be provided by a high photocatalyst concentration, excessive C/TiO_2 will lead to much higher turbidity in the solution and provide a shielding effect for the lighting, thus weakening the degradation capacity.[36] Meicen Guo *et al.* also demonstrated that the scarring of light to the photocatalyst would be raised by an overdose of CNTS–TiO_2.[37] In view of the energy and efficiency, a favorable 1 g L^{-1} C/TiO_2 was adopted in our tests.

3.2.4 Effect of the pH. The pH of a solution has a crucial impact on the photocatalytic performance. To test this, 1 g L^{-1} C/TiO_2 was added into 100 mL NH_3–N solution (50 mg L^{-1}), and the photocatalytic reaction was carried out under a xenon lamp (AM1.5, 25 A) for 1 h. The solution pH was adjusted in the range of pH 3–11 by adding 1 M HCl or NaOH. During the reaction, samples were taken out and filtered at set time intervals, and the NH_3–N concentration of the supernatant was then analyzed.

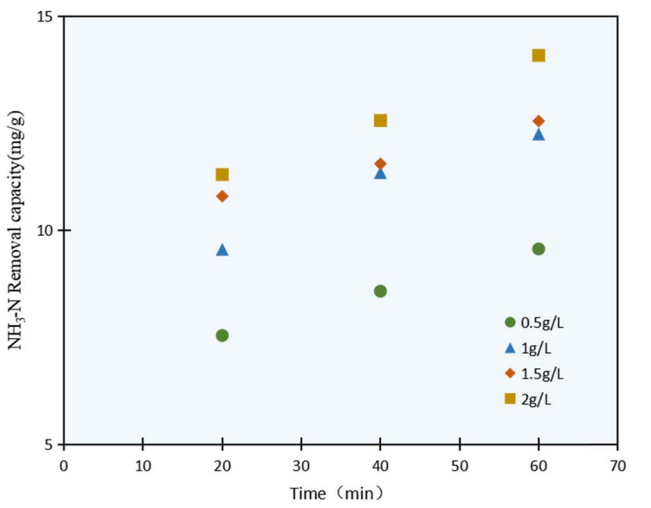

Fig. 4 NH_3–N removal capacity with various C/TiO_2 dosages (AM1.5, 25 A, pH 10.0, C_0 = 50 mg L^{-1}).

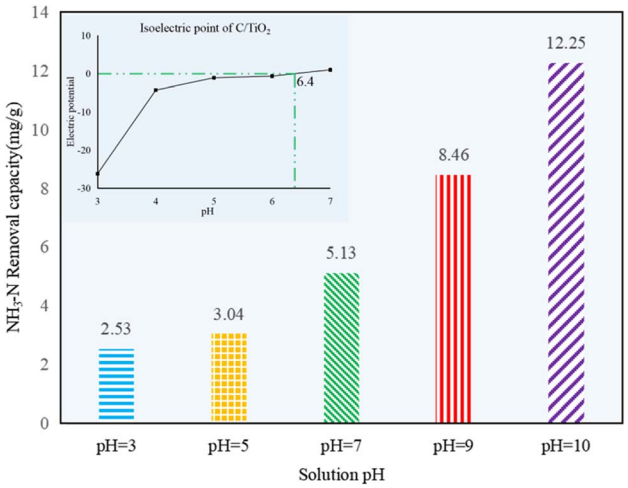

Fig. 5 NH_3–N removal capacity at different initial solution pH values (AM1.5, 25 A, 1 g L^{-1} C/TiO_2, C_0 = 50 mg L^{-1}).

As shown in Fig. 5, the NH_3–N removal capacity was strongly affected by the solution pH, and it increased obviously with the pH changing from acid to alkaline. Compared to the control group 1 in Fig. 1, there was no efficient NH_3–N removal by photocatalysis in acid conditions, as noted by the very limited reduction in the NH_3–N amount (less than 3.04 mg g^{-1}, which was lower than the 4.46 mg g^{-1} of the control group). However, the NH_3–N removal capacity was *ca.* 4 or 5 times higher at pH 10.0 than the ones in acidic solution, indicating the photocatalysis performed better under alkaline conditions.

The surface charge of the photocatalyst and the existing form of NH_3–N in water can seriously be affected by the solution pH. Negative charges appeared on the photocatalyst under alkaline conditions. Here, the OH^- concentration was increased while H^+ concentration was decreased with pH increasing, and more $^{\bullet}OH$ would be excited by C/TiO_2 under light irradiation, so the removal capacity of NH_3–N on C/TiO_2 was improved.[10] Besides, NH_4^+ and NH_3 are two forms of N in NH_3–N solution. More NH_3 appeared as the pH increased. Satoshi Shibuya *et al.* found that it was much more efficient for photocatalysis when ammonia existed in the molecular form, and NH_3–N removal capacity would be more prominent when mainly molecular ammonia existed.[38] The pH_{pzc} of C/TiO_2 was around 6.4 (Fig. 5). Thus, the photocatalyst had positive charges on its surface when the solution pH was lower than its pH_{pzc} and displayed negative charges when the solution pH was higher than 6.4. Ammonia can be much easier gathered onto the C/TiO_2 surface by electrostatic attraction in alkaline solution, while it could hardly be attracted to C/TiO_2 under acidic condition. However, Marco Altomare *et al.* confirmed that the NH_3–N removal rate would decrease at pH higher than 10.5 due to the competitive adsorption of hydroxide anions on the surface of the photocatalyst.[39] Thus, the NH_3–N removal capacity was much better in an appropriate alkaline environment (pH 10.0).[4]

3.3 Characterization

3.3.1 SEM-EDS and BET. As shown in Fig. 6, C/TiO_2 displayed an irregular granular and obvious porous structure compared to commercial TiO_2. The porous biochar in C/TiO_2 enhanced its ability to attract NH_3–N around the C/TiO_2 for better photocatalytic reaction.[22] Besides, C/TiO_2 had more pores and a bigger specific surface area than raw biochar according to our previous research, which are favorable for enhancing the NH_3–N photocatalytic degradation.[40] According to the analysis of the EDS data, the C wt% in C/TiO_2 was *ca.*17.6% higher than that of pure TiO_2, while the Ti wt% in C/TiO_2 was 61.0% lower than that of the commercial TiO_2. These indicate that the introduction of biochar on TiO_2 was successful and stable. Table 2 lists the EDS results for TiO_2, biochar, and C/TiO_2, confirming Si, Fe, and other elements were successfully introduced in C/TiO_2 after biochar modification, which enhanced its photocatalytic ability.[41–43]

The N_2 adsorption/desorption isotherms of C/TiO_2 are shown in Fig. 7, where it can be seen there was a hysteresis loop at a relative pressure (P/P_o) ranging from 0.6 to 0.85, which illustrated that the biochar-modified TiO_2 exhibited a typical type-IV isotherm with the existence of a mesoporous structure. From the calculated BET data, the proportion of mesopores was over 90% and the specific surface area of the C/TiO_2 photocatalyst increased from 11.88 (pure TiO_2) to 119.47 $m^2\ g^{-1}$ after modification, which was about 9 times higher than that of the pure TiO_2. The inset in Fig. 7 shows the pore-size distribution for C/TiO_2 and pure TiO_2, showing that the pure TiO_2 had little mesoporous structure, while the proportion of the mesoporous structure in C/TiO_2 was significantly enhanced, and the total pore volume of C/TiO_2 also showed

Table 2 EDS results for TiO_2, biochar, and C/TiO_2[a]

Element	TiO_2 (wt%)	Biochar (wt%)	C/TiO_2 (wt%)
C	2.86	11.67	20.46
O	18.53	7.44	17.47
Ti	78.62	—	17.62
Si	—	1.89	3.80
Fe	—	0.65	0.41
Zn	—	16.93	1.40
Other	—	61.42	38.84

[a] C in commercial TiO_2 might arise from the impurities during measurement, while the Au in C/TiO_2 was from the gold-spraying treatment.

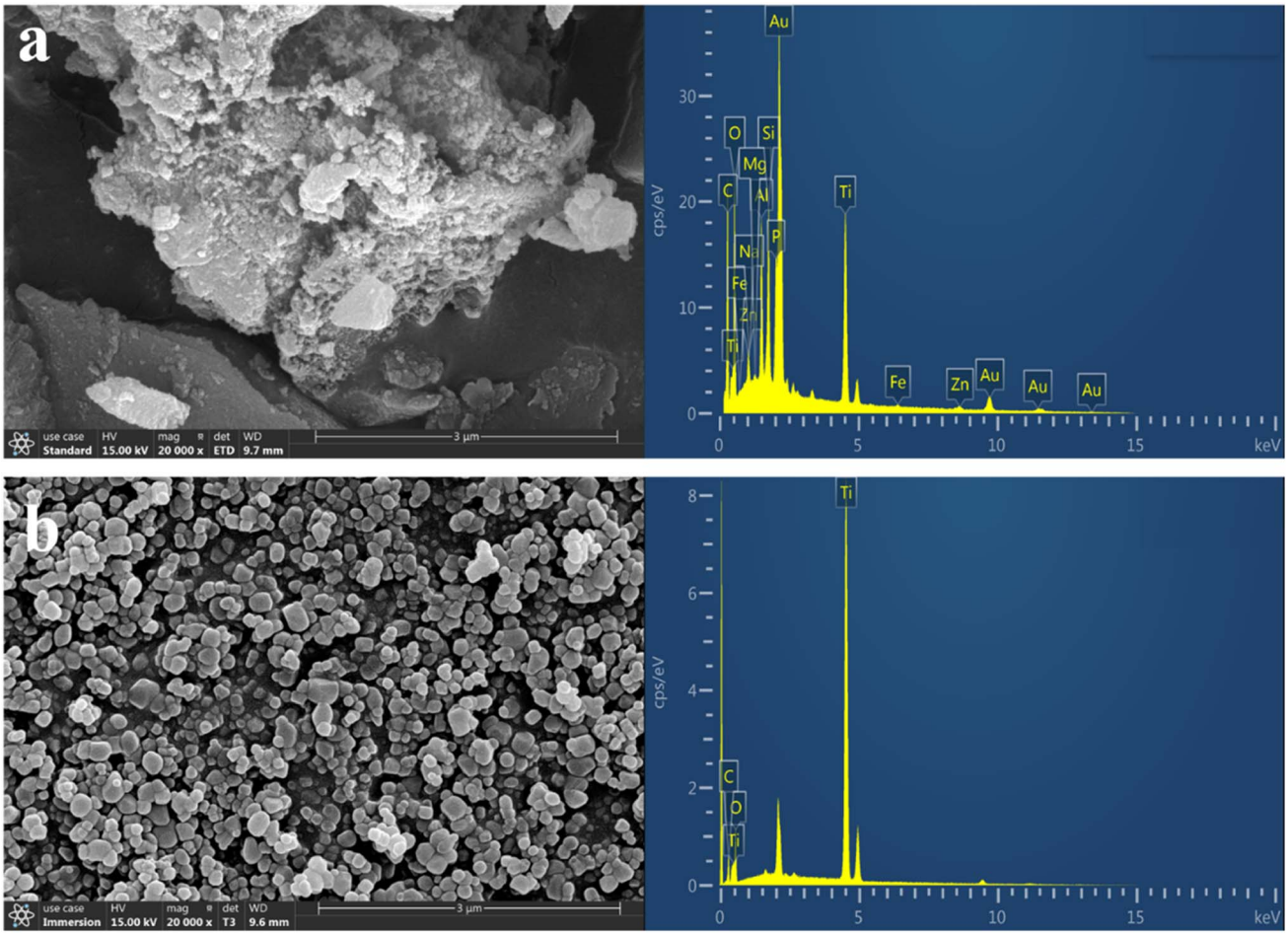

Fig. 6 SEM-EDS analysis for C/TiO_2 and TiO_2 (a) C/TiO_2; (b) TiO_2.

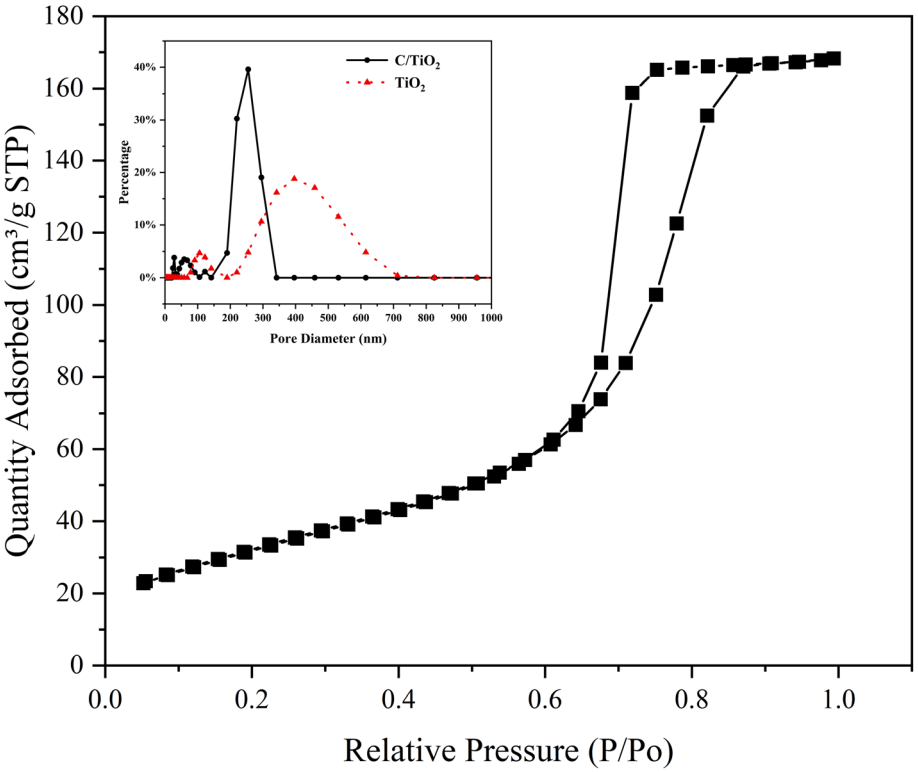

Fig. 7 N_2 adsorption/desorption isotherms of C/TiO_2 and the pore-size distribution curves of TiO_2 and C/TiO_2.

a remarkable increase. This indicated that the porous structure and pore volume of TiO_2 could be effectively enhanced after biochar modification. Thus, C/TiO_2 had a more developed pore structure, which made the composite material have a larger specific surface area and more contact area and active points with pollutants.

3.3.2 XRD. XRD spectroscopy of the typical anatase-TiO_2, rutile-TiO_2, and the composed C/TiO_2 was performed and the

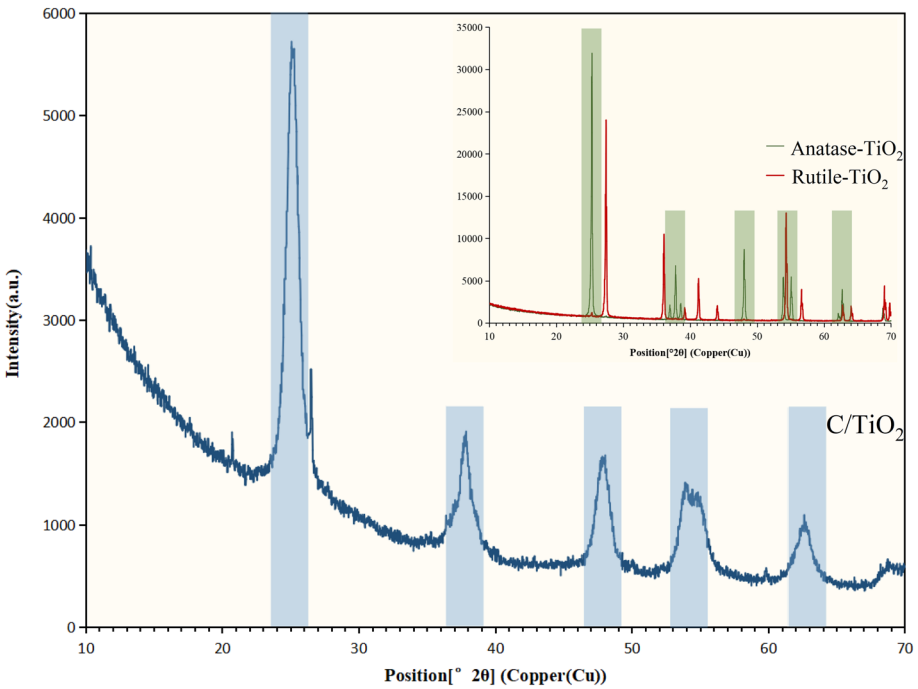

Fig. 8 XRD spectra for C/TiO_2, anatase-TiO_2, and rutile-TiO_2.

spectra are shown in Fig. 8. The standard rutile-TiO_2 has characteristic peaks at $2\theta = 27.4°$, 36.1°, 41.2°, 44.0°, 54.3°, 56.6°, and 64.0° (PDF#21-1276), respectively, while a typical anatase-TiO_2 has characteristic peaks at $2\theta = 25.3°$, 37.8°, 48.0°, 53.9°, and 62.7° (PDF#21-1272), respectively. As shown in Fig. 8, the produced C/TiO_2 had characteristic peaks at $2\theta =$ 25.1°, 37.8°, 47.8°, 53.9°, and 62.7°, respectively, which were roughly consistent with those of a typical anatase-TiO_2. Due to the lab synthesis, there were slight differences in terms of a superior quality and uniformity between the produced TiO_2 and commercial TiO_2, and a minor blue-shift was noted on the composed C/TiO_2 as compared to the pure TiO_2. Moreover, some small peaks appeared in C/TiO_2 that were possibly generated from impurities in the biochar. Though the size growth of TiO_2 nanocrystals was slightly inhibited due to the introduction of the biochar, TiO_2's phase structure was unaffected. C/TiO_2 still presented a remarkable anatase structure and good photocatalysis performance. Moreover, the results

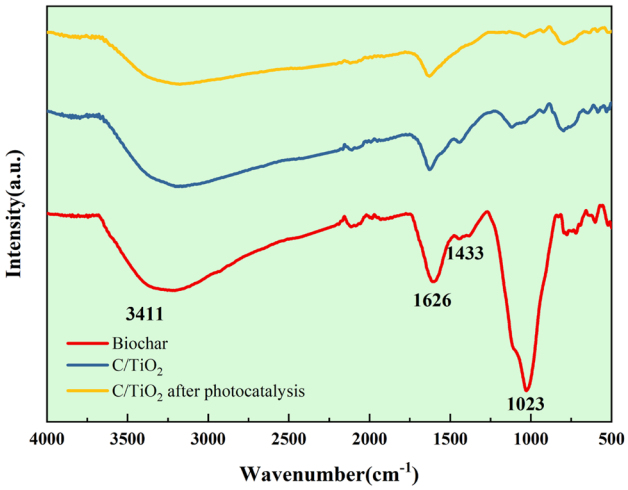

Fig. 10 FT-IR spectra of C/TiO_2 and biochar.

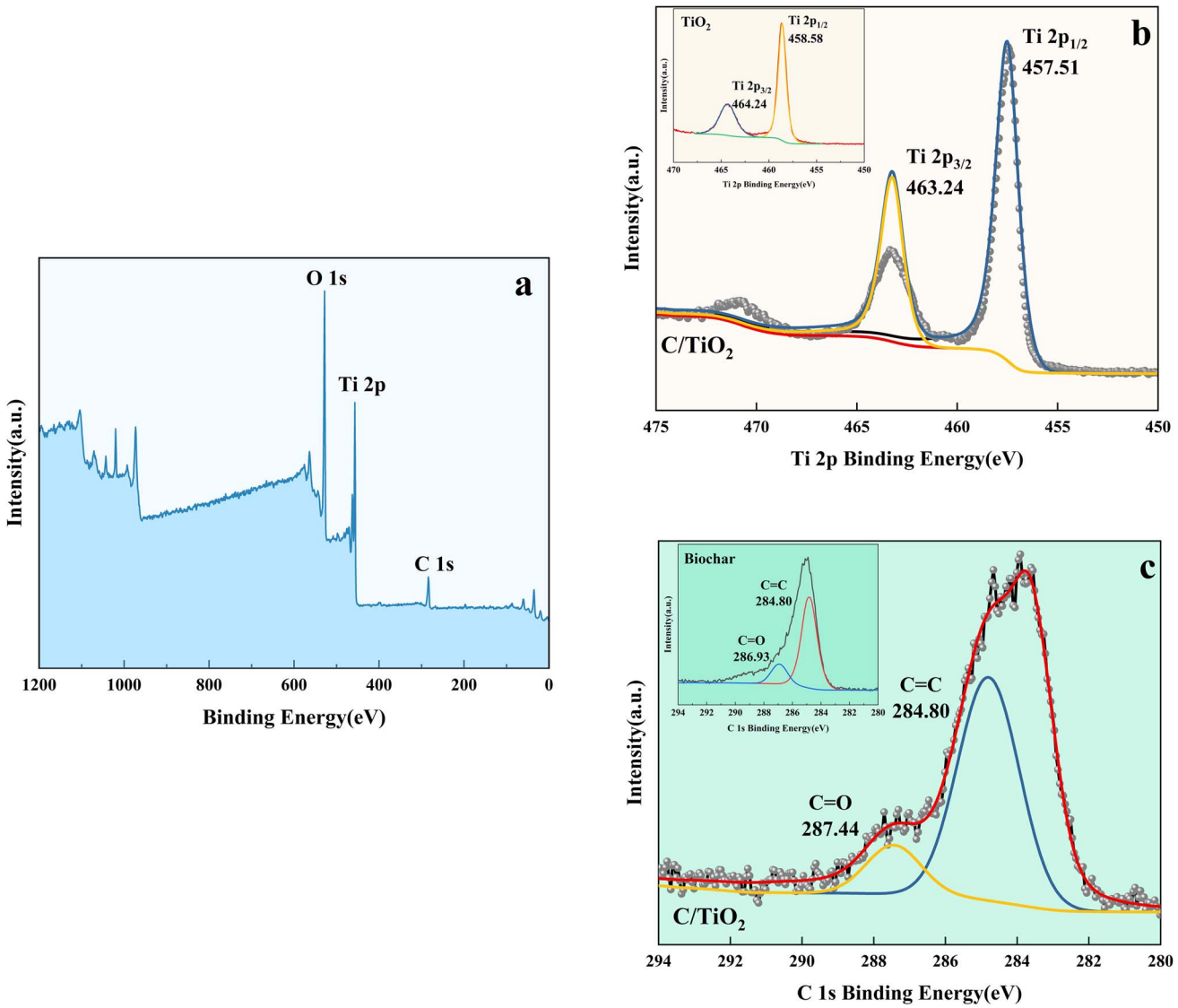

Fig. 9 XPS spectra of C/TiO_2 (a), Ti 2p in C/TiO_2 and biochar (b), and C 1s in C/TiO_2 and biochar (c).

demonstrated that biochar and TiO_2 were combined successfully.[28]

3.3.3 XPS. Fig. 9 shows the XPS spectrum of C/TiO_2. The full survey spectrum of C/TiO_2 is shown in Fig. 9a, and the high-resolution Ti, C spectra are shown in Fig. 9b and c. All the binding energy values were calibrated against the C 1s at 284.8 eV.[8]

As shown in Fig. 9b, the Ti 2p peaks at 457.51 and 463.24 eV were related to Ti $2p_{1/2}$ and Ti $2p_{3/2}$ of Ti^{4+}, respectively. Compared to the typical TiO_2, the binding energy was reduced slightly on C/TiO_2 because of the introduction of biochar, which might cause low-load electrons to transfer from the TiO_2 surface to the biochar surface. Thus, the outer layer electron-distribution density of TiO_2 was changed, leading to a reduction of the binding energy. As shown in Fig. 9c, C 1s peaks

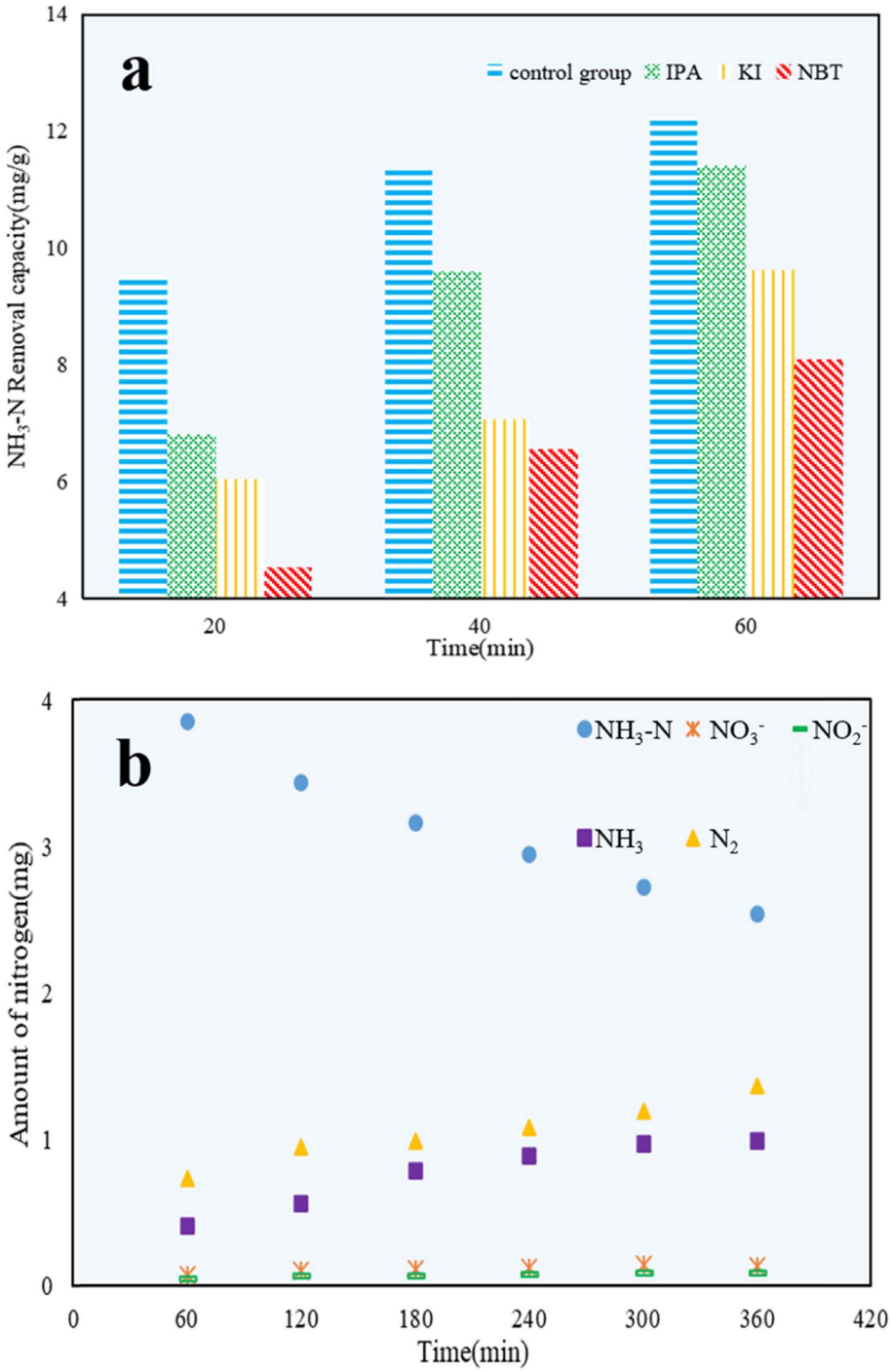

Fig. 11 NH_3–N removal capacity under different quenching agents (a), and plot of the amounts of NH_3–N, NO_3^-, NO_2^-, NH_3, and N_2 in the reaction system (b) (AM1.5, 25 A, 1 g L^{-1} C/TiO_2, pH 10.0, C_0 = 50 mg L^{-1}).

appeared at 284.80 and 287.44 eV corresponding to C $1s_{3/2}$ and C $1s_{1/2}$, respectively. The peak was slightly shifted from 286.93 eV on biochar to 287.44 eV on C/TiO_2 due to the combination between TiO_2 and biochar. The high C content in C/TiO_2 changed its hydrophilicity and resulted in an increment in C=O groups. Then, the introduction of biochar was beneficial to $^{\bullet}OH$ formation, which could form oxygen vacancies on the composed photocatalyst.[44] Thus, more oxygen was attracted to C/TiO_2, consequently improving its photocatalytic performance. In conclusion, the introduction of biochar was effective for enhancing the NH_3–N removal efficiency of the composite.

3.3.4 FT-IR. Fig. 10 shows the infrared spectra of the photocatalysts and biochar, which were used to analyze the surface functional group characteristics of the composite. As shown in Fig. 10, the spectra of the three materials were similar. Obviously, the peaks at 1023, 1433, and 1626 cm^{-1} were weaker in C/TiO_2 before and after the photocatalysis in comparison with biochar. The peaks around 1023 cm^{-1} were assigned to C–O and C–O–C stretching.[45] Moreover, hydroxyl groups (–OH) were also confirmed by the peaks around 1023 cm^{-1}, which are usual in hybrid materials prepared from municipal sewage sludges.[46] Compared to the original biochar, the strength of the peak at 1023 cm^{-1} on C/TiO_2 was lowered probably due to the very small amount of biochar in the final composite product. The peaks at 1433 cm^{-1} were attributed to –COO–Ti vibration.[31] The peaks at 1626 cm^{-1} indicated the antisymmetric stretching vibration of $^{\bullet}OH$ groups and peaks formed by surface moisture through stretching and bending.[47] The peaks at 3411 cm^{-1} were generated from the stretching vibrations of the active –OH or –COOH groups. Owing to the successful C-modification from biochar, a large amount of carboxyl groups (–COOH) was present on the surface of the C/TiO_2 composite, which further intensified the interactions between biochar and TiO_2.[48]

3.4 Mechanism

Propan-2-ol (IPA),[49] potassium iodide (KI),[50] and nitro blue tetrazolium (NBT)[51] were added to NH_3–N solutions to explore the effect of hydroxyl radicals ($^{\bullet}OH$), valence band holes (h^+), and superoxide radicals ($^{\bullet}O_2^-$) on the photocatalytic reactions, respectively. As shown in Fig. 11a, the photocatalytic efficiency of C/TiO_2 was restrained compared with the control group, which confirmed that h^+, $^{\bullet}OH$, and $^{\bullet}O_2^-$ all had certain impacts on the NH_3–N removal capacity. After 60 min, the NH_3–N removal capacity of C/TiO_2 under NBT addition was 8.10 mg g^{-1}, which was clearly lower than for both cases with IPA and KI addition. It was demonstrated that $^{\bullet}O_2^-$ played a major role in NH_3–N degradation, while both $^{\bullet}OH$ and h^+ had effects on NH_3–N removal to some extent too.[52]

Next, 1 g L^{-1} C/TiO_2 was added into 100 mL of 50 mg L^{-1} NH_3–N solution (pH 10.0), and the photocatalytic reaction was carried out under a xenon lamp (AM1.5, 25 A) with stirring (450 rpm) for 6 h. The amount of NO_3^-, NO_2^-, and NH_3 were measured every 1 h, and the amount of N_2 generated was calculated *via* the conservation of mass.

As shown in Fig. 11b, the amounts of NH_3–N, NO_3^-, NO_2^-, NH_3, and N_2 during the NH_3–N photocatalytic reaction were calculated and compared. The stable decrease in the amount of NH_3–N illustrated the continuous photocatalytic degradation of NH_3–N. Because of the high pH, NH_3 became the main form of NH_3–N in water. Thus, the increased content of NH_3 was attributed to ammonia blowing off from the solution during the experiments. After 6 h, the amount of NO_3^- and NO_2^- detected was tiny and could be ignored. The amount of N_2 was much larger than NO_3^- and NO_2^-, and was almost 2 times higher than that of NH_3. This proved that NH_3–N was mainly converted to the non-noxious N_2. C/TiO_2 was effective in the photocatalytic reaction and was shown to be a significant method to treat low-concentration NH_3–N solutions.[53]

4. Conclusions

An advanced C/TiO_2 composite photocatalyst using solid waste was prepared by the sol–gel method for the effective and environmentally friendly degradation of NH_3–N in aqueous solutions. The removal capacity of NH_3–N on the composite was higher than that on commercial TiO_2 at pH 10 with 1 g L^{-1} C/TiO_2 under both 60 and 120 min irradiation (xenon lamp, AM1.5, 25 A). The photocatalytic efficiency of C/TiO_2 under simulated sunlight irradiation displayed good performance and its NH_3–N removal capacity increased with the light power increasing, while NH_3–N removal by C/TiO_2 was favorable in a proper alkaline environment (pH 10.0).

The characterization of C/TiO_2 through SEM-EDS, BET, XRD, XPS, and FT-IR showed the successful introduction of biochar onto TiO_2. As shown in the SEM-EDS and BET analysis, C/TiO_2 had a larger surface area and more pores compared to the raw materials. XRD spectroscopy showed that C/TiO_2 had similar characteristic peaks with anatase-TiO_2, which indicated that the biochar addition did not change TiO_2's effective phase structure. Compared to TiO_2, some carbon- and oxygen-containing functional groups were presented in C/TiO_2 that originated from the biochar modification, and effectively proved its photocatalytic performance by the XPS and FT-IR results. According to the radical quenching experiment and NH_3–N photocatalytic degradation analysis, superoxide radicals ($^{\bullet}O_2^-$) were proved to be the main oxidant influencing the removal capacity, and N_2 was the main product of the photocatalytic reaction. Compared to commercial anatase-TiO_2, C/TiO_2 displayed a relatively higher efficiency for NH_3–N removal, but also had more significance for beneficial solid-waste utilization. This work could provide an economic and meaningful photocatalyst to treat NH_3–N wastewater. In future research, studies should focus on further improvement of the photocatalytic efficiency, and sustainable utilization and practical application tests should be carried out.

Author contributions

Jiawei Wang: experiment, data curation, formal analysis, writing – original draft, visualization. Guoqiao Wang: conceptualization, methodology, experiment. Tian Yu: data curation,

writing – original draft, experiment. Nengjie Ding: experiment. Meicheng Wang: experiment. Yao Chen: supervision, methodology, writing – reviewing and editing, visualization.

Conflicts of interest

There are no conflicts to declare.

Acknowledgements

The authors declare that no funds, grants, or other support were received during the preparation of this manuscript.

Notes and references

1 Ministry of Ecology and Environment of the People's Republic of China, *Annual Report of China's Ecological and Environmental Statistics*, 2020.
2 A. R. Brown, M. Lilley, J. Shutler, C. Lowe, Y. Artioli, R. Torres, E. Berdalet and C. R. Tyler, *Rev. Aquacult.*, 2019, **12**, 1663–1688.
3 A. Damar, K.-J. Hesse, F. Colijn and Y. Vitner, *Deep Sea Res., Part II*, 2019, **163**, 72–86.
4 X. Luo, C. Chen, J. Yang, J. Wang, Q. Yan, H. Shi and C. Wang, *Int. J. Environ. Res. Public Health*, 2015, **12**, 14626–14639.
5 D. Qu, D. Sun, H. Wang and Y. Yun, *Desalination*, 2013, **326**, 135–140.
6 A. Alshameri, A. Ibrahim, A. M. Assabri, X. Lei, H. Wang and C. Yan, *Powder Technol.*, 2014, **258**, 20–31.
7 M. Sakar, R. Mithun Prakash and T. Do, *Catalysts*, 2019, **9**, 680.
8 L. Lu, R. Shan, Y. Shi, S. Wang and H. Yuan, *Chemosphere*, 2019, **222**, 391–398.
9 Y. M. Hunge, A. A. Yadav, A. G. Dhodamani, N. Suzuki, C. Terashima, A. Fujishima and V. L. Mathe, *Ultrason. Sonochem.*, 2020, **61**, 104849.
10 M. Pelaez, N. T. Nolan, S. C. Pillai, M. K. Seery, P. Falaras, A. G. Kontos, P. S. M. Dunlop, J. W. J. Hamilton, J. A. Byrne, K. O'Shea, M. H. Entezari and D. D. Dionysiou, *Appl. Catal., B*, 2012, **125**, 331–349.
11 R. Yu, X. Yu, J. Fu, Y. Zhang, Y. Liu, Y. Zhang and S. Wu, *Water Environ. J.*, 2021, **35**, 962–970.
12 L. Deng, B. Chang, D. Shi, X. Yao, Y. Shao, J. Shen, B. Zhang, Y. Wu and X. Hao, *Renewable Energy*, 2021, **170**, 858–865.
13 Z. Liu, J. Qiu, C. Zheng and L. Li, *AIP Conf. Proc.*, 2017, **1820**, 030004.
14 M. Nasr, C. Eid, R. Habchi, P. Miele and M. Bechelany, *ChemSusChem*, 2018, **11**, 3023–3047.
15 Y. Jia, P. Liu, Q. Wang, Y. Wu, D. Cao and Q. A. Qiao, *J. Colloid Interface Sci.*, 2021, **585**, 459–469.
16 W. Shi, S. Yang, H. Sun, J. Wang, X. Lin, F. Guo and J. Shi, *J. Mater. Sci.*, 2020, **56**, 2226–2240.
17 W. Shi, K. Shu, H. Sun, H. Ren, M. Li, F. Chen and F. Guo, *Sep. Purif. Technol.*, 2020, **246**, 116930.
18 C. H. A. Tsang, K. Li, Y. Zeng, W. Zhao, T. Zhang, Y. Zhan, R. Xie, D. Y. C. Leung and H. Huang, *Environ. Int.*, 2019, **125**, 200–228.
19 X. Xiao, B. Chen, Z. Chen, L. Zhu and J. L. Schnoor, *Environ. Sci. Technol.*, 2018, **52**, 5027–5047.
20 P. D. Dissanayake, S. You, A. D. Igalavithana, Y. Xia, A. Bhatnagar, S. Gupta, H. W. Kua, S. Kim, J.-H. Kwon, D. C. W. Tsang and Y. S. Ok, *Renewable Sustainable Energy Rev.*, 2020, **119**, 109582.
21 S. Fan, Y. Wang, Z. Wang, J. Tang, J. Tang and X. Li, *J. Environ. Chem. Eng.*, 2017, **5**, 601–611.
22 L. Zhang, P. Ma, L. Dai, S. Li, W. Yu and J. Guan, *Catal. Sci. Technol.*, 2021, **11**, 3834–3844.
23 L. He, G. Wang, X. Zhang, Y. Zhang and Y. Chen, *Water Sci. Technol.*, 2020, **82**, 1643–1652.
24 G. Wang, J. Wang, T. Yu, X. Guo and Y. Chen, *RSC Adv.*, 2022, **12**, 31966–31975.
25 F. Dalanta and T. D. Kusworo, *Chem. Eng. J.*, 2022, **434**, 134687.
26 M. Zendehzaban, M. Ashjari and S. Sharifnia, *Int. J. Energy Res.*, 2019, **44**, 2150–2163.
27 Y. Shavisi, S. Sharifnia, S. N. Hosseini and M. A. Khadivi, *J. Ind. Eng. Chem.*, 2014, **20**, 278–283.
28 Q. Zhou, H. Yin, A. Wang and Y. Si, *Chin. J. Chem. Eng.*, 2019, **27**, 2535–2543.
29 S. Wang, Q. Xu, Y. Zhang, G. Jin, W. He and N. Zhang, *Rev. Roum. Chim.*, 2020, **65**, 789–794.
30 X. Peng, M. Wang, H. Dai, F. Qiu and F. Hu, *Environ. Sci. Pollut. Res. Int.*, 2020, **27**, 39198–39210.
31 J. Feng, X. Zhang, G. Zhang, J. Li, W. Song and Z. Xu, *Chemosphere*, 2021, **274**, 129689.
32 Z. Shayegan, C.-S. Lee and F. Haghighat, *Chem. Eng. J.*, 2018, **334**, 2408–2439.
33 T. Le Thi Thanh, L. Nguyen Thi, T. Tran Dinh and N. Nguyen Van, *J. Chem.*, 2019, **2019**, 1–8.
34 H.-Y. Cheng, K.-C. Chang, K.-L. Lin and C.-M. Ma, *AIP Conf. Proc.*, 2018, **1946**, 020006.
35 W. Wang, G. Li, D. Xia, T. An, H. Zhao and P. K. Wong, *Environ. Sci.: Nano*, 2017, **4**, 782–799.
36 D. Chen, Y. Cheng, N. Zhou, P. Chen, Y. Wang, K. Li, S. Huo, P. Cheng, P. Peng, R. Zhang, L. Wang, H. Liu, Y. Liu and R. Ruan, *J. Cleaner Prod.*, 2020, **268**, 121725.
37 M. Guo, X. Yu, J. Liu, L. Wang, Z. Nie and H. Yang, *IOP Conf. Ser.: Mater. Sci. Eng.*, 2018, **301**, 012138.
38 S. Shibuya, Y. Sekine and I. Mikami, *Appl. Catal., A*, 2015, **496**, 73–78.
39 M. Altomare, G. L. Chiarello, A. Costa, M. Guarino and E. Selli, *Chem. Eng. J.*, 2012, **191**, 394–401.
40 P. Lisowski, J. C. Colmenares, O. Mašek, W. Lisowski, D. Lisovytskiy, A. Kamińska and D. Łomot, *ACS Sustainable Chem. Eng.*, 2017, **5**, 6274–6287.
41 N. Bao, Z. Wei, Z. Ma, F. Liu and G. Yin, *J. Hazard. Mater.*, 2010, **174**, 129–136.
42 D. Channei, B. Inceesungvorn, N. Wetchakun, S. Ukritnukun, A. Nattestad, J. Chen and S. Phanichphant, *Sci. Rep.*, 2014, **4**, 5757.

43 Y. Pan, Y. Zhang, Y. Huang, Y. Jia, L. Chen and H. Cui, *J. Hazard. Mater.*, 2021, **416**, 125802.
44 Y. Zhou and M. Sun, *Environ. Sci. Pollut. Res. Int.*, 2022, **29**, 12261–12281.
45 S. Au-pree, P. Narakaew, S. Thungprasert, T. Promanan, A. Chaisena and S. Narakaew, *Eng. J.*, 2021, **25**, 53–68.
46 J. Matos, M. Rosales, A. García, C. Nieto-Delgado and J. R. Rangel-Mendez, *Green Chem.*, 2011, **13**, 3431–3439.
47 C. F. Carbuloni, J. E. Savoia, J. S. P. Santos, C. A. A. Pereira, R. G. Marques, V. A. S. Ribeiro and A. M. Ferrari, *J. Environ. Manage.*, 2020, **262**, 110347.
48 X. U. Zu-Shun, Z. Quan-Yuan, H. U. Xiao-Yu, L. Guang-Fu and P. Qiu-Hu, *J. Inorg. Mater.*, 2019, **34**, 219–224.
49 L. Sun, Y. Zhou, X. Li, J. Li, D. Shen, S. Yin, H. Wang, P. Huo and Y. Yan, *Chin. J. Catal.*, 2020, **41**, 1573–1588.
50 Y. Li, H. Sun, T. Peng, H. You, Y. Qin and L. Zeng, *Appl. Clay Sci.*, 2019, **179**, 105155.
51 X. Jia, Z. Shen, Q. Han and H. Bi, *Chin. J. Catal.*, 2022, **43**, 288–302.
52 M. S. S. Dorraji, M. H. Rasoulifard, H. Daneshvar, A. Vafa and A. R. Amani-Ghadim, *J. Mater. Sci.: Mater. Electron.*, 2019, **30**, 12152–12162.
53 J. Feng, X. Zhang, G. Zhang, J. Li, W. Song and Z. Xu, *Chemosphere*, 2021, **274**, 129689.